Multiple Phase Screen Calculation of Two-way Spherical Wave Propagation in the Ionosphere

Dennis L. Knepp
NorthWest Research Associates
301 Webster Street
Monterey, CA 93940
(e-mail: dennis.knepp@nwra.com)

Abstract

This paper presents a numerical solution to the parabolic wave equation for spherical wave propagation in a disturbed ionosphere. The solution uses the Fourier/split step approach where the propagation medium is modeled using multiple phase-changing screens separated by free space. The phase screens can consist of deterministic or random components describing spatial scales of any size. This solution consists of realizations of the signal (i.e., the ionospheric transfer function) after two-way propagation from a transmitter, through the medium to a target, and back. The target can be comprised of multiple, independent point scatterers. The solution is applicable to many propagation problems including synthetic aperture radar and is not subject to the small scene limitation, where all scatterers in the scene experience identical propagation conditions. Several examples are given illustrating some features of the solution including reciprocity, relationship between one- and two-way (monostatic and bistatic) scintillation index, and reflection from a large target.

Introduction

A number of researchers are interested in the possibility of a space-based wide bandwidth synthetic aperture radar (SAR). *Carrano et al.* [2012] develop a three-dimensional split step propagation simulation to consider ionospheric disturbances on PALSAR L-band imagery. This work utilizes plane wave propagation and makes the small-scene approximation. In a paper dealing with a proposed P-band SAR, *van de Kamp et al.* [2009] consider the impact of variations of total electron content on SAR imaging performance. The present paper describes a highly accurate method to generate realizations of the propagating signal for the case of two-way propagation of a spherical wave through a disturbed ionosphere and back. The solution does not require the small-scene approximation and calculates realizations that intrinsically exhibit the spatial correlation imposed after two-way propagation. In related work *Gherm et al.* [2005] compute realizations of signals after 3D spherical-wave propagation using Rytov's approximations for the correlation of the real and imaginary parts of the propagating signal. Their realizations have characteristics determined by the moment equations. In contrast, the MPS technique is based directly on the in-situ ionospheric structure with no intervening analytic calculations. The work of *Carrano et al.* [2012] applies to 3D plane waves propagating at a fixed angle with respect to a phase screen.

Formulation

In this section we describe the theory to allow for spherical wave propagation using multiple phase screen techniques where the propagating medium is subdivided into a series of phase-changing screens separated by free space. The scalar Helmholtz equation for a propagating spherical wave can be written as follows [*Yeh and Liu*, 1977].

$$\nabla^2\psi + k^2(1+\beta\epsilon)\psi \;\; = \;\; 0 \tag{1}$$

where

$$\beta = \frac{-\omega_p^2}{\omega^2 - \omega_p^2}; \qquad \epsilon = \frac{\Delta N_e}{\langle N_e \rangle}; \qquad k = \frac{2\pi}{\lambda} \tag{2}$$

In (2) $\omega_p^2 = 4\pi c^2 r_e \langle N_e \rangle$, where r_e is the classical electron radius, $\langle N_e \rangle$ is the mean electron density, and ΔN_e is the deviation in electron density. The symbol k is the wavenumber and c is the speed of light in a vacuum. In the following we will assume that $\omega \gg \omega_p$. Let the propagating wavefront have the form

$$\psi(x,y,z) = \frac{U(x,y,z)}{(z-z_t)} \times \exp\left\{-ik\left(z - z_t + \frac{(x-x_t)^2 + (y-y_t)^2}{2(z-z_t)}\right)\right\} \tag{3}$$

which is the Fresnel-region or parabolic approximation for a spherical wave that originates at (x_t, y_t, z_t) and propagates in the positive z direction. Here the time dependence $\exp(i\omega t)$ is suppressed. Assume the propagation distance is large and substitute the expression for ψ into (1) to obtain the equation for $U(x,y,z)$. Next make the substitutions:

$$\theta = \frac{(x-x_t)}{z'}; \qquad \phi = \frac{(y-y_t)}{z'}; \qquad z' = z - z_t \tag{4}$$

and ignore higher order terms in $1/(z-z_t)$ to obtain a simplified expression for $U(\theta, \phi, z')$ given by

$$\left(\frac{1}{z'^2}\right)\left(\frac{\partial^2 U}{\partial\theta^2} + \frac{\partial^2 U}{\partial\phi^2}\right) - i2k\frac{\partial U}{\partial z'} + k^2\beta\epsilon U = 0 \tag{5}$$

Consider for convenience only the two-dimensional problem, corresponding to infinitely elongated irregularities in the y-direction, with only θ and z' variation. This geometry is appropriate for propagation in the earth's equatorial region. Now separate the thick ionized layer into a number of thin layers, each of which is modeled as a central phase changing screen (phase screen) surrounded by free space.

Propagation through a phase screen

Consider a layer of thickness $\Delta z'$ centered at zero z'. For small $\Delta z'$ the equation for propagation through this layer is obtained from (5) with the first (diffraction) term neglected. Recognizing that the deviation in the index of refraction is $\Delta n = 2\pi k^2 r_e \Delta N_e$ and using (2), one can describe the effect of the phase screen as

$$U\left(\theta, \frac{\Delta z'}{2}\right) = U\left(\theta, \frac{-\Delta z'}{2}\right) \exp\left\{-ik\int_{\frac{-\Delta z'}{2}}^{\frac{\Delta z'}{2}} \Delta n(\theta,\zeta)\, d\zeta\right\} \tag{6}$$

Free space propagation

Equation (5) is valid for free-space propagation between the phase screens if the last term is neglected. To solve the resulting equation, introduce the Fourier transform

$$\hat{U}(q_\theta, z') = \int_{-\infty}^{\infty} U(\theta, z') \exp(-i2\pi q_\theta \theta) d\theta \tag{7}$$

and its inverse transform. The solution for free-space propagation from z_1' to z_2' is

$$\hat{U}(q_\theta, z_2') = \hat{U}(q_\theta, z_1') \exp\left\{\frac{i2\pi^2 q_\theta^2}{k}\left(\frac{1}{z_1'} - \frac{1}{z_2'}\right)\right\} \tag{8}$$

The solution for the electric field is then obtained using (8) to propagate from screen to screen and (6) to propagate through each phase screen. This simply involves a series of Fourier transforms that are implemented numerically using fast Fourier transforms (FFTs).

Propagation geometry

For simplicity, consider the basic propagation geometry shown in Figure 1 similar to that of a ground based radar observing a target through the natural ionosphere. The transmitter or transmitters are located in the plane $z = 0$, the ionosphere is described by five phase screens around $z = 200$ km, and the targets (or point reflectors) are located in the plane $z = 600$ km. For down-going propagation, the signal propagates from the plane of the targets back to the transmitter plane $z = 0$. For two-way propagation, the propagating wave reflects as a spherical wave from each of the point reflectors in the target plane, and propagates down to the plane $z = 0$. In the following, the plane $z = 0$ is referred to as the receiver plane for down-going propagation. There can be any number of transmit, target (reflector), and receiver locations in a calculation, and these need not be coincident. In the examples below, we use several different configurations of transmitters, targets, and receivers.

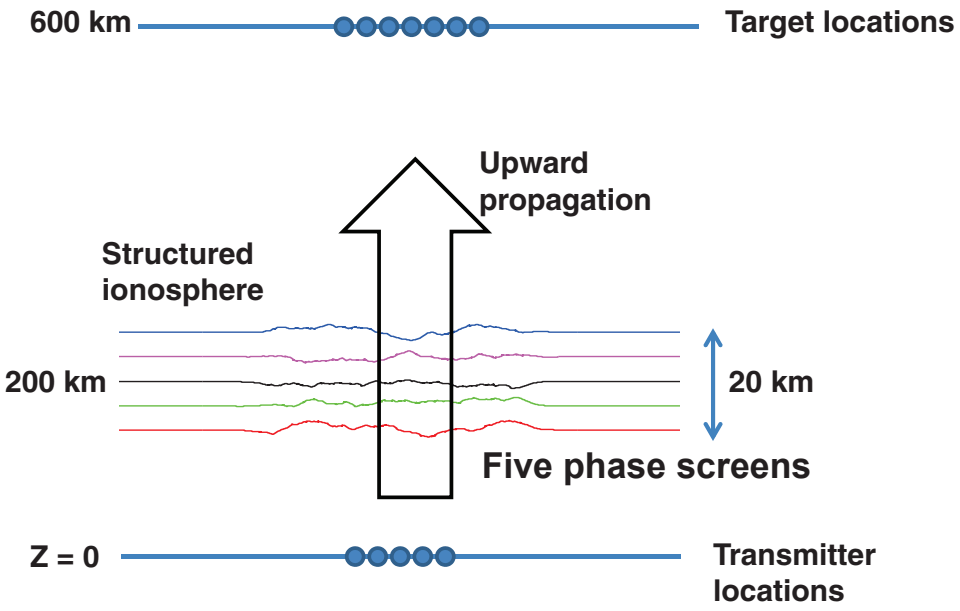

Figure 1: Propagation geometry for one-way up-going propagation from transmitters located at $z = 0$, through phase screens located near $z = 200$ km, to targets (or scatterers) located at $z = 600$ km. For down-going propagation, the wave originates at $z = 600$ km and propagates through the same phase screens to the plane $z = 0$ km.

Two-way propagation

Let the number of transmitters be N_{xmtr}, the number of point-reflector targets be N_{tar}, and the number of receivers be N_{rcvr}. Then write the voltage at all the transmitter locations as a row vector with a dimension of $1 \times N_{xmtr}$. For up-going propagation from the transmitter

plane to the target plane, the voltage at the N_{tar} point reflectors along the MPS x-axis in the target plane is written as

$$V(x, z_{tar}) = V(x, z_{xmtr}) G_{up}(xmtr \rightarrow tar) \tag{9}$$

The Green's function matrix has dimensions $N_{xmtr} \times N_{tar}$ so that $V(tar)$ has dimensions $1 \times N_{tar}$. Similarly, for down-going propagation from the target plane back to the receiver plane

$$\begin{aligned} V(x, z_{rcvr}) &= V(x, z_{tar}) G_{down}(tar \rightarrow rcvr) & (10) \\ &= V(x, z_{xmtr}) G_{up}(xmtr \rightarrow tar) G_{down}(tar \rightarrow rcvr) & (11) \end{aligned}$$

where (11) is obtained by combing (9) and (10). The two-way Green's function $G_{up}G_{down}$ is a matrix of size $N_{xmtr} \times N_{rcvr}$.

In the numerical propagation simulation, we generate the Green's function matrix using a single transmitter location and all desired target locations, then we proceed to the next transmitter location, generating a row of the Green's function matrix in each MPS calculation. The phase screens do not change during these calculations, but interpolation is required because the transmitter is moved to the center of the MPS calculation grid for each simulation. Since all the phase screens then need to shift accordingly, this process generally requires interpolation along the screens. The Green's function for downward propagation is generated similarly. Once both Green's function are calculated, post processing can be applied to calculate the two-way fields due to any desired combinations of transmitters and scatterers. This process is particularly useful for synthetic aperture radar evaluation for two reasons. First, the scatterers can have any desired reflectivity and thus model objects in a scene. Secondly, this implementation of two-way propagation does not require the "small-scene" approximation. That is, radar returns originating from different points in the scene propagate through different parts of the ionosphere with the proper amount of decorrelation. The MPS code calculates the quantity $U(x, y, z)$ in (3). The exponential term in (3) is applied in post processing to obtain two-way fields from extended transmitters or reflectors. The z term in the denominator is ignored in the examples below. *Knepp*, [1983] discusses the requirements for grid length, spacing of points in the grid, etc.

Scintillation index

In the following examples, we utilize the MPS code to calculate one- and two-way propagation examples. We consider two-way (radar) propagation where the up- and down-paths are either identical (monostatic radar) or independent (bistatic radar). In either case, the severity of fluctuations in power due to ionospheric propagation is characterized by the S_4 scintillation index.

For one-way propagation, S_4(one-way) is defined through

$$S_4^2(\text{one-way}) = \frac{\langle (s - \langle s \rangle)^2 \rangle}{\langle s \rangle^2} \tag{12}$$

where the quantity s is the power due to fluctuations solely in the ionospheric propagation channel. For one-way propagation, assume that the probability density function of the power s in the received electric field is well-modeled by the Nakagami-m probability density function

$$p(s) = \frac{m^m s^{m-1}}{\Gamma(m) \langle S \rangle^m} \exp\left\{ \frac{-ms}{\langle S \rangle} \right\}, \; s \geq 0, \; \text{(one-way)} \tag{13}$$

where the angle brackets denote statistical averages. The mean one-way power is $\langle S \rangle$ and the value of the one-way scintillation index is calculated as $S_4^2(\text{one-way}) = 1/m$ [*Knepp and Houpis,* 1991; *Fremouw and Ishimaru,* 1992].

From these two references, one can obtain the relationship between S_4(one-way) and the scintillation index for two-way monostatic and two-way bistatic propagation. These relationships are

$$S_4^2(\text{monostatic}) = S_4^2(\text{one-way}) \left(\frac{4 + 6S_4^2(\text{one-way})}{1 + S_4^2(\text{one-way})} \right) \quad (14)$$

$$S_4^2(\text{bistatic}) = S_4^2(\text{one-way}) \left(2 + S_4^2(\text{one-way}) \right) \quad (15)$$

Examples

We applied the formalism described above to create several examples of results from this two-way propagation simulation. For simplicity, we used only a simple propagation geometry, similar to that of a ground based radar observing a target through the natural ionosphere. This geometry is shown in Figure 1 for up-going propagation paths. The transmitter is located at $z = 0$, the ionosphere is described by a single phase screen at $z = 200$ km (or by five phase screen centered at $z = 200$ km), and the target is located in the plane $z = 600$ km. For down-going propagation, the signal propagates from the plane of the targets/reflectors back to the transmitter plane. There can be any number of transmit, target, and receiver locations in a calculation. In the examples below, we use several different configurations of transmitters, targets, and receivers, determined by their locations along the x-axis.

The phase screens which contain the information on ionospheric structure, all consist of 2^{19}, or 524,288 points in the x-direction. The transmission frequency is 300 MHz. Each screen consists of two basic components, a random phase based on a power-law power spectral density, with outer scale of 5 km, inner scale of 10 m, and one-dimensional slope of 3, corresponding to a K^{-4} slope for in-situ electron density (where K is the wavenumber). The amplitude of the phase screens is controlled by the parameter σ_ϕ. The MPS calculation here is performed using both the $x - z$ and the $\theta - z'$ coordinate systems. The phase screens are computed in the $x - z$ plane and their lengths are calculated for up-going propagation according to $L_i = (z_i - z_{xmtr})\theta_{max}$ where θ_{max} is an input parameter fixed here as unity, L_i is the screen length, z_{xmtr} gives the transmitter location, and z_i is the location of the ith phase screen. The phase screens are one-dimensional and are generated along the x coordinate of the MPS grid. Figure 2 shows an example of the phase of five phase screens for one of the calculations where each phase screen has $\sigma_\phi = 10$ rad. The free-space propagation calculation is performed in $\theta - z$ coordinates according to (8). As the wave propagates up and away from the transmitter, the resolution in the x-dimension decreases.

We actually implemented the down-going propagation step in this code, although this is not necessary unless the ionosphere changes rapidly during the time it takes for a wave to propagate from the transmitter to the target and back. Otherwise, one would need only to perform the up-going propagation step and reciprocity could be used to relate down-going propagation to up-going. For the explicit down-going propagation step, different length phase screens are generally needed than those for up-going propagation. But the phase of the phase screen does not change (unless the ionosphere changes). To handle this situation of both up- and down-going propagation, we calculated the required length of all phase screens for both propagation directions and picked the maximums. Before performing the propagation steps,

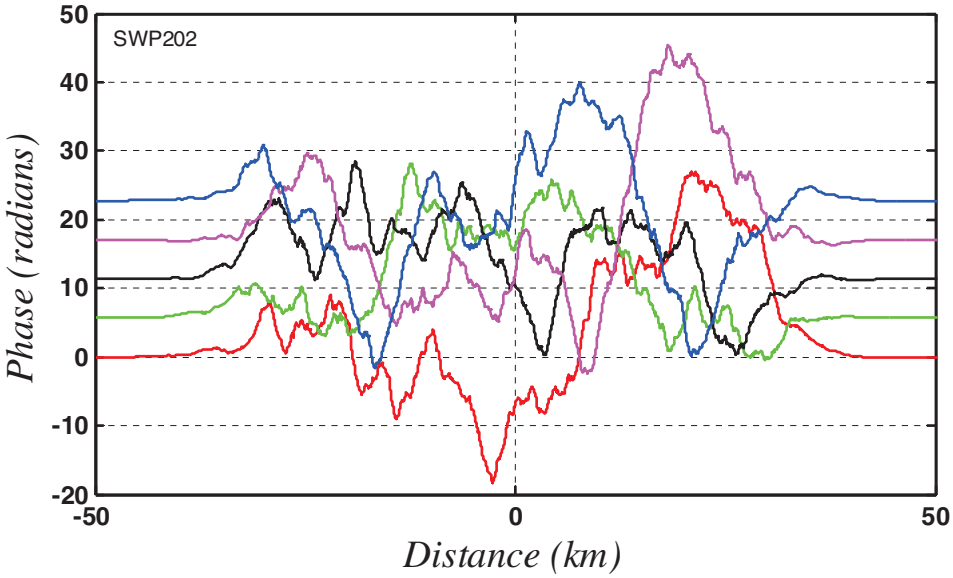

Figure 2: The phase of the five phase screens for outgoing propagation, plotted on the same scale offset by 6 radians with respect to one another. The screens are located at $z = 190, 195, 200, 205,$ and 210 km, respectively. The phase screens are all around 200 km in length. Only a small portion of the grid is shown.

we calculated and stored the phase of all the phase screens. While performing the propagation calculation from screen-to-screen, we interpolate in x so that we could evaluate the phase at equally spaced values of θ throughout the entire up- or down-going calculation.

In the examples herein, the phase screens are all around 200 km in length, so that the spacing between points that comprise the phase screens is around 0.4 meters or less. Since this spacing is much less than the 10-meter inner scale size, the minimum size of the phase fluctuations is determined by the inner scale, not the spacing of the points in the MPS grid.

Example 1: Reciprocity

It is important that the numerical propagation calculation satisfy reciprocity in which the received field remains the same if the location of the receiver and transmitter are interchanged. As a check, we calculated two examples using the same geometry shown in Figure 1, one with five phase screens (each screen has a σ_ϕ of 10 radians), and one with a single phase screen where σ_ϕ is 22.4 radians. Figure 3 shows an I-Q plot of the one-way fields as a smooth green curve for up-going propagation from a single transmitter to 4001 target locations extending covering 4000 m along the MPS grid in the target plane and separated by one meter in the x-direction. The plot gives the amplitude and phase of the field for all 4001 target locations as points connected by straight line segments. If there were no scintillation, the figure would show a circle of radius unity. The fields for down-going propagation from these same 4001 target locations and back to a single receiver located at $x = 0, z = 0$ are shown as discrete small red circles. To make the plot useful, only every fifteenth point for down-going propagation is shown. Reciprocity holds to a very high degree of accuracy for this case of five phase screens, with similar results for the case of one phase screen. We also considered the case of 4001 transmitters, 4001 targets, and 4001 receivers, calculating the field for all possible up-and down-going paths. We then measured the maximum difference in the amplitude of all possible reciprocal paths.

For both cases of one and five phase screens the maximum difference in the magnitude of the complex field was about 3×10^{-5}.

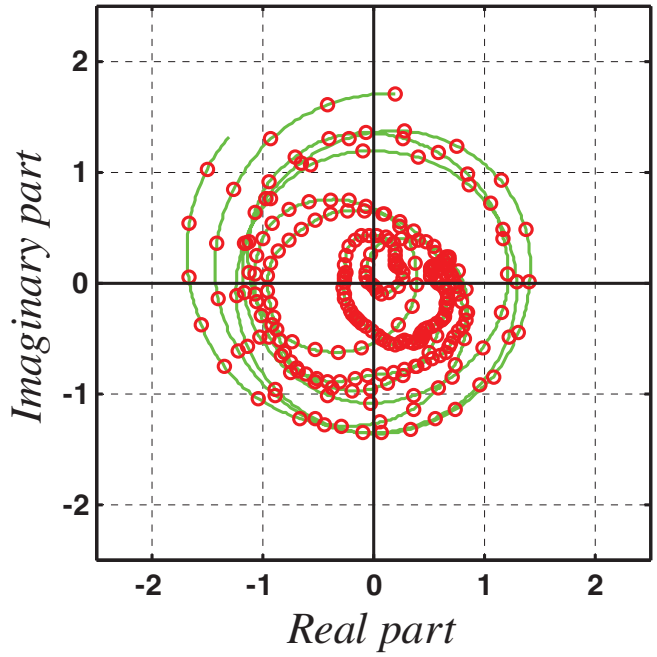

Figure 3: Comparison of the complex voltages for reciprocal propagation paths for up- and down-going propagation for the case of five phase screens centered near $z = 200$ km.

Example 2: Two-way scintillation index

We used two separate propagation geometries to measure the scintillation index after one-way and two-way, monostatic and bistatic propagation. A single transmitter is located at $x = 0$ in the transmit plane. In the target plane we used 4001 targets, centered in the x-axis in the target plane, and separated by 5 m. The target objects extend over a distance of 20 km in the x-direction. To measure the value of S_4(up) we applied (12), taking the averages over the one-way field at the 4001 target locations. For two-way monostatic propagation, the single receiver in the plane $z = 0$ is located at $x = 0$. For two-way bistatic propagation, the single receiver is located at $x = 4$ km, $z = 0$. To measure the value of S_4(two-way) we applied (12) to the two-way field after propagation from the single transmitter, up to 4001 targets (or reflectors), then back down to a single receiver.

Figure 4 compares the MPS simulation results to the theory above. Each point in the figure represents the result of a separate MPS calculation, with different random phase screens and σ_ϕ. For weak scattering, where one-way scintillation index (S_4(up)) is less than 0.5, the simulation and theory agree very well. As the scintillation severity increases, the numerical values for monostatic S_4 agree with the theory. For bistatic S_4, the agreement between simulation and theory is still quite good, with a tendency for the simulation points to lie below the theoretical curve.

Example 3: Two-way propagation

This example illustrates the effect of ionospheric structure on the antenna pattern of a long scatterer consisting of discrete omnidirectional elements. Let a single transmit element

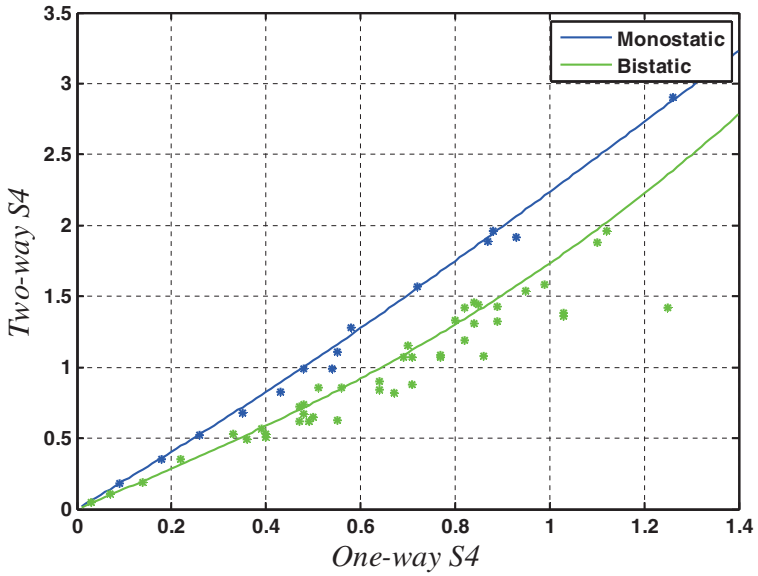

Figure 4: Comparison of analytic (smooth curves) and simulation results for the relationship between one- and two-way scintillation indices for the cases of monostatic (blue) and bistatic (green) radar.

at $x = 0$ illuminate an array of 401 reflectors located in the target plane. The reflectors are separated by $\lambda/2 = 0.5$ m and have a total length of 200 m. The same five phase screens described in the previous examples cause scintillation in the propagating wavefront. The field from the 401 reflectors propagates back down to many locations in the receive plane. We consider two cases here with different levels of ionospheric disturbance. In the less severe case, each of the five phase screens has $\sigma_\phi = 4$ radians. The resulting one-way value of $S_4(\text{up}) = 0.16$. In the more severe case, each of the five phase screens has $\sigma_\phi = 12.5$ radians with resulting $S_4(\text{up}) = 0.46$.

The top frames in Figures 5 show the two-way power in the receiver plane after scattering from the 401 reflectors. The field expected for the case of no ionospheric disturbance is calculated analytically and shown for comparison. On the left, for weak scattering, the power deviates only a little due to the ionospheric structure. On the right, for stronger scattering, the two-way field deviates significantly from that expected for no scintillation. The field varies peak-to-peak by 10 dB or so, and the nulls in the undisturbed scattering pattern are largely filled in. Because the received field consists of the contribution from many, decorrelated reflectors, the peak-to-peak fluctuations in power are reduced in comparison to the case of a single reflector. These top frames are essentially the radiation pattern versus distance for the large linear aperture. The distance subtended by the "main-beam" is close to the commonly used value of $(z_{tar} - z_{xmtr})\lambda/D = 3$ km, where the antenna length, D is 200 m.

The second frame shows the phase across a 20-km portion of the receiver plane. Because of the large propagation distances involved, the phase is quite large and differences between the disturbed and undisturbed cases are not evident. The third frame shows the phase deviation between the phase with no disturbance and that with disturbances. On the right, for weak scattering, the phase deviations are largest when the amplitude goes through a null.

The bottom frame shows the angle-of-arrival (AoA) at the receiver plane as a function of distance along the MPS grid. The AoA is measured by sliding a 10-meter antenna consisting of multiple elements along the receive plane and applying the well-known correlation technique [*Therrien*, 1992], which is optimal in white noise. (There is no noise in these examples.) In

the bottom frame on the right, the AoA is zero at $x = 0$, where the propagation is straight downwards. In both weak and moderate fading, the AoA fluctuations are most evident in the areas of nulls in the antenna pattern where the signal is smallest, which is expected. For stronger scattering, there is substantially more variation in AoA throughout the 20-km portion of the MPS grid shown. Note that the total computational length of the MPS grid at the receiver is 600 km.

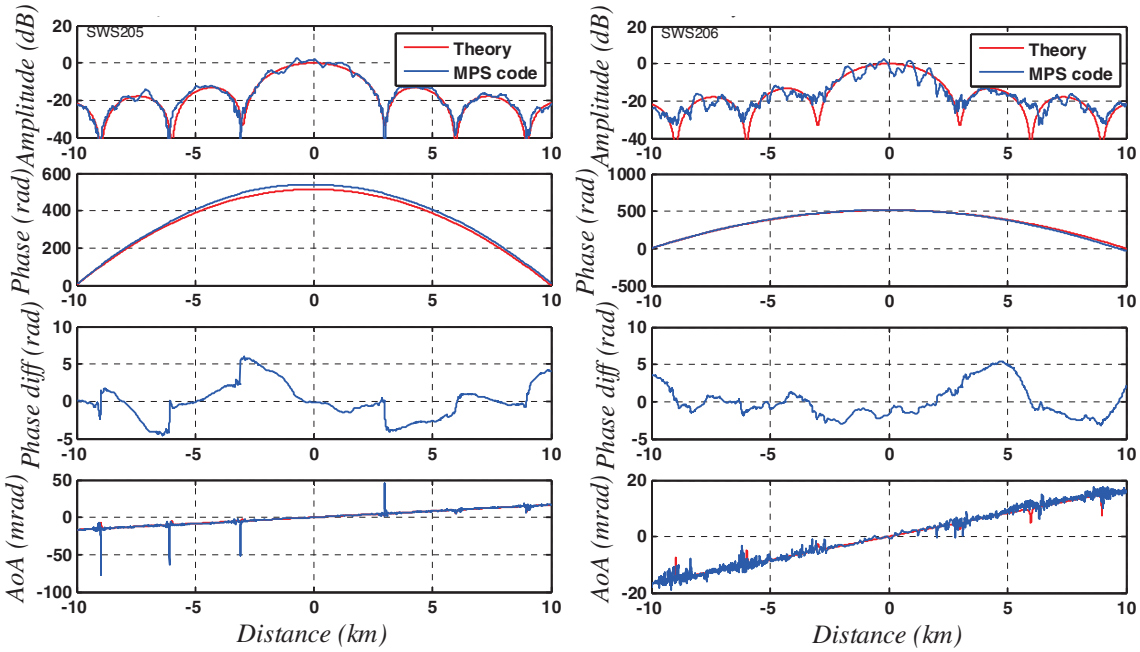

Figure 5: Amplitude, total phase, detrended phase, and angle-of-arrival after two-way propagation through five phase screens. There is a single transmitter, 401 targets spaced by $\lambda/2$ at $z = 600$ km, and many receive locations. On the right, each screen has $\sigma_\phi = 4.0$ radians and $S_4(\text{up}) = 0.16$. On the left, each screen has $\sigma_\phi = 12.5$ radians and $S_4(\text{up}) = 0.46$. The smooth red curve shows the same quantities for the case of no ionospheric irregularities.

Conclusions

Use of the parabolic wave equation is a very accurate approach to solve for a propagating EM wave in structured ionization. This work develops a multiple phase screen (MPS) approach for two-way propagation of spherical waves. The MPS solution is quite general, and may be easily applied to problems involving numerous, separated, layers of ionization, characterized either by deterministic-like specifications or by spatially-varying power spectral density. MPS techniques can handle all levels of ionospheric disturbances from the least severe, where only minor phase fluctuations occur, to the most severe cases of frequency-selective scintillation. The present paper is limited to the case of two-dimensional propagation, where the irregularities are infinite in the y-direction. This is a good model of the earth's equatorial region. The extension to 3D propagation is straightforward.

The work here is a useful step towards the goal of understanding and mitigating the effects of the ionosphere on space based synthetic aperture radar. Implementation of two-way propagation allows for targets that can have any desired level of reflectivity and thus can be

used to describe realistic scenes. The propagation solution here does not invoke the small scene approximation and enables a realistic evaluation of the effects of ionospheric propagation.

References

Carrano, C. S., K. M. Groves, and R. G. Caton (2012), Simulating the impacts of ionospheric scintillation on L-band SAR image formation, *Radio Sci.*, 47, RS0L20, doi:10.1029/2011RS004956.

Fremouw, E. J., and A. Ishimaru (1992), Intensity scintillation index and mean apparent radar cross section on monostatic and bistatic paths, *Radio Sci.*, 27(4), 539543, doi:10.1029/92RS00293.

Gherm, V. E., N. N. Zernov, and H. J. Strangeways (2005), Propagation model for transionospheric fluctuating paths of propagation: Simulator of the transionospheric channel, *Radio Sci.*, 40, RS1003, doi:10.1029/2004RS003097.

Knepp, D. (1983), Multiple phase-screen calculation of the temporal behavior of stochastic waves, *Proc. IEEE*, 71, 722737.

Knepp, D. L., and H. L. F. Houpis (1991), Altair VHF/UHF/ observations of multipath and backscatter enhancement, *IEEE Trans. Antennas Propag.*, 39(4), 528534, doi:10.1109/8.81467.

Therrien, C. W. (1992), Discrete random signals and statistical signal processing, Prentice-Hall, Inc, New Jersey.

van de Kamp, M., P. S. Cannon, and M. Terkildsen (2009), Effect of the ionosphere on defocusing of space-based radars, *Radio Sci.*, 44, RS1003, doi:10.1029/2007RS003808.

Yeh, K. C., and C. H. Liu (1977), An investigation of temporal moments of stochastic waves, *Radio Sci.*, 12(5), 671680, doi:10.1029/RS012i005p00671.

Zernov, N. N., V. E. Gherm, and H. J. Strangeways (2012), Further determinations of strong scintillation effects on GNSS signals using the Hybrid Scintillation Propagation Model, *Radio Sci.*, 47, RS0L06, doi:10.1029/2011RS004935.

Acknowledgement

This work was supported under contract FA8718-09-C-0001 from the Air Force Research Laboratory. The enthusiastic support of Drs. William Borer and Keith Groves, and Mr. Ron Caton are gratefully acknowledged.